Structure of ^{12}N using ^{11}C+p resonance scattering

K. Peräjärvi,[1,*] Changbo Fu,[2] G. V. Rogachev,[3] G. Chubarian,[2] V. Z. Goldberg,[2] F. Q. Guo,[1,4] D. Lee,[1,5] D. M. Moltz,[4]
J. Powell,[1] B. B. Skorodumov,[6] G. Tabacaru,[2] X. D. Tang,[2] R. E. Tribble,[2] B. A. Brown,[7] A. Volya,[3] and Joseph Cerny[1,4]

[1]*Nuclear Science Division, Lawrence Berkeley National Laboratory, Berkeley, California 94720, USA*
[2]*Texas A&M University, Cyclotron Institute, College Station, Texas 77843, USA*
[3]*Physics Department, Florida State University, Tallahassee, Florida 32306, USA*
[4]*Department of Chemistry, University of California, Berkeley, California 94720, USA*
[5]*Department of Nuclear Engineering, University of California, Berkeley, California 94720, USA*
[6]*University of Notre Dame, Notre Dame, Indiana 46556, USA*
[7]*Michigan State University, East Lansing, Michigan 48824, USA*

The level structure of ^{12}N has been investigated from 2.2 to 11.0 MeV in excitation energy using a ^{11}C+p resonance interaction with thick targets and inverse kinematics. Excitation functions were fitted using an R-matrix approach. Sixteen levels in ^{12}N were included in the analysis, several of them are new. Spin-parity assignments, excitation energies and widths are proposed for these levels.

I. INTRODUCTION

The level structure of the drip-line nucleus ^{12}N has been studied in the past using conventional beams; see Ref. [1] and references therein. More recent references [2,3] are basically extensions of those earlier works. Interest in the nuclear structure of ^{12}N (and ^{12}B) is primarily related to the idea that many low-lying levels in ^{12}N (and ^{12}B) should manifest one-particle-one-hole configurations, and therefore their features provide a test (and parameters) for shell-model calculations. In the past, ^{12}B was more accessible than ^{12}N and therefore several relatively low-lying levels, which are known in ^{12}B, have not yet been identified in ^{12}N. However, ^{12}N is more unstable to single-particle decay than ^{12}B. Therefore, the nucleon widths of the levels in ^{12}N could provide direct information on their single-particle structure.

In addition to the nuclear physics interest, studies involving ^{12}N around its ^{11}C+p threshold at 0.601 MeV are often also driven by nuclear astrophysics interests [4–8]. Namely, to be able to accurately determine the astrophysical rate of the ^{11}C$(p, \gamma)^{12}$N reaction, detailed knowledge of the low-lying level structure of ^{12}N is also required. The ^{11}C$(p, \gamma)^{12}$N reaction is associated with hot pp chains that might be able to bypass the triple α process in producing CNO material in low-metallicity stars [9]. The ^{12}N excitation region in the vicinity of the ^{8}B+α threshold at 8.008 MeV is also important for astrophysics because of the formation of ^{11}C in the ^{8}B(α, p) reaction [9]. Favorable states in ^{12}N close to this threshold could strongly enhance the corresponding reaction rate. The ^{8}B$(\alpha, p)^{11}$C reaction has been experimentally studied in Ref. [10]. That measurement was done using the inverse kinematics reaction, i.e., it utilized a radioactive ^{11}C beam. Resonant states between 8.7 and 9.9 MeV in ^{12}N were probed, and no resonant structures were reported.

As a result of these past studies, we can conclude that the level structure in ^{12}N is relatively well established up to the first 3^- state at 3.13 MeV. The present work extends our knowledge of the level structure of ^{12}N by covering the excitation energy interval from 2.2 to 11.0 MeV. States within this energy interval were populated using ^{11}C+p resonance scattering.

The first part of the experimental results to be reported were obtained using the Berkeley Experiments with Accelerated Radioactive Species (BEARS) coupled cyclotron system [11], which provided ^{11}C beams of 2×10^7 ions/s on target. This beam was used with a solid target. The second part of the experimental data was obtained at Texas A&M University (TAMU) with the magnetic separator MARS [12] with beams of 10^6 ions/s on a gas target.

II. EXPERIMENTAL SETUP AND RESULTS AT LBNL

These experiments required two different setups and two ^{11}C beam energies to cover the 2.2- to 11.0-MeV excitation energy interval.

A. The ^{11}C beam

In the BEARS system a 40-μA, 10-MeV proton cyclotron was used as a driver accelerator, producing ^{11}C, which was then transported as CO_2 and injected into the Advanced ECR ion source (AECR-U) [13] of the Lawrence Berkeley National Laboratory's (LBNL) 88-inch cyclotron. Radioactive ^{11}C ($T_{1/2} = 20.4$ min) nuclei were synthesized via (p, α) reactions on a nitrogen gas target. To produce the CO_2 about 0.2% O_2 was added to the target gas. During the ^{11}C beam preparation cycle, the proton beam was first on for 5 min, after which irradiated gas was unloaded into a holding tank where it could be kept for a minute or two to let part of the ^{14}O ($T_{1/2} = 70.6$ s), which is also produced, to decay away. After unloading, the target chamber was refilled with the nitrogen-oxygen gas mixture and the production cycle was repeated.

*Present address: Department of Physics, University of Jyväskylä, Finland.

From the holding tank the activity was transported in helium gas about 350 m into the 88-in. cyclotron building using a capillary technique [14]. The $^{11}CO_2$ was cryogenically separated from the helium and injected into the AECR-U ion source. The ^{11}C beam was extracted from the ion source in its 4+ charge state, where it has the maximum efficiency of 11% [11].

The $^{11}C^{4+}$ beam was accelerated using the 88-in, cyclotron to 90 and 125 MeV, respectively. However, because of its low intensity, the cyclotron and the beam line optics had to be first tuned on a phosphorous plate at the target position using stable 180 and 250 MeV $^{22}Ne^{8+}$ analog beams. Then the phosphorous plate was replaced with a thin target (Au, 1.5 mg/cm^2) which was observed by a particle-identification telescope setup and the cyclotron frequency was set to accelerate trace amounts of $^{11}B^{4+}$ (always present in the source). After ^{11}B identification with the telescope, $^{11}CO_2$ was let into the AECR-U ion source. Because the cyclotron frequency difference between $^{11}B^{4+}$ and $^{11}C^{4+}$ is only 1.4 kHz, they could not be resolved because the cyclotron frequency resolution for these beam energies is between 5 and 7 kHz. However, the ^{11}B component of the beam could be eliminated using a stripper foil (Al, 204 μg/cm^2)/bending magnet combination upstream of the target. The magnets were set so that only the fully stripped $^{11}C^{6+}$ ions were able to reach the target with a typical $^{11}C^{6+}$ beam intensity of 2×10^7 ions/s. Because this is enough intensity to be weakly seen with a sensitive phosphorous plate, the plate was returned to the target position to perform the final focusing of the beam.

B. The setup for the 2.2- to 6.6-MeV excitation energy interval

The experiments at both excitation energy regions used a 60-in. scattering chamber. This chamber is equipped with a rotatable target ladder and two arms for detectors, all remotely controlled [15]. In addition to the above mentioned phosphorous plate and the gold scattering foil, the target ladder held a 12.4-mg/cm^2-thick nickel degrader followed by a 18.4-mg/cm^2-thick $(CH_2)_n$ (= polyethylene) foil and a similar 12.4-mg/cm^2 nickel degrader followed by a 28.0-mg/cm^2-thick carbon foil, for background measurements. Higher beam intensities on target could be obtained by accelerating $^{11}C^{4+}$ to 90 MeV on first harmonic and then reducing it to the desired ~73.8 MeV by the aluminum stripper and the nickel degrader. Measurements at $0°$ were made possible by using the thick target inverse kinematics (TTIK) method [16]. In addition to $0°$ data, measurements at $15°$ in the laboratory were also carried out. This approach lets us probe the elastic-scattering excitation function from about 2.2 to 6.6 MeV in ^{12}N simultaneously. The TTIK technique relies on the large difference in energy loss between ^{11}C and the elastically scattered proton in the $(CH_2)_n$ target. The proton background originating from the $^{11}C+^{nat}Ni$, ^{nat}C reactions was evaluated by bombarding the nickel degrader-carbon target combination at the same energy.

A ΔE (thickness 72 μm)-E (thickness 3 mm) Si-detector telescope was mounted on one scattering chamber arm, about 14.6 cm away from the target, behind a circular collimator with a diameter of about 18.1 mm. This Si telescope was also used during the ^{11}C beam tuning. The VME-based data acquisition system recorded coincidences between the E and ΔE detectors. The energy calibration of the detectors was done using the elastically scattered protons and the resonant protons from the well-known states in ^{12}N at 2.439(9) MeV (0^+) and 3.132(8) MeV (3^-) [1,6] (see also Sec. VI A below). The experimental energy resolution was about 35 keV in the center-of-mass frame.

C. The setup for the 6.5- to 11.0-MeV excitation energy interval

To study the states around the $^8B+\alpha$ threshold at 8.008 MeV (from 6.5 to 11.0 MeV) in ^{12}N with the $^{11}C+p$ elastic and inelastic resonance scattering, a 125 MeV ^{11}C beam was employed. In this experiment plain 20.2 and 44.3-mg/cm^2-thick $(CH_2)_n$ foils were used as the targets. The ^{11}C beam was not stopped in the thinner polyethylene target, preventing measurements at $0°$. Its main purpose was to provide the non-$0°$ excitation energy functions above 8.6 MeV, which were not covered by the TAMU experiment discussed in Sec. III. It also permitted direct studies of the inelastic component of the scattering for the states near the $^8B+\alpha$ threshold. To evaluate the proton background originating from the $^{11}C+^{nat}C$ reactions when using the $(CH_2)_n$ targets, a 27.0-mg/cm^2-thick carbon foil was bombarded at the same beam energy.

To look at states up to 11 MeV in inverse kinematics, we needed to detect protons with energies up to about 38 MeV, requiring a Si-detector telescope with a minimum thickness of about 7.5 mm. To be able to go even further than that (important for background subtraction), the following detector configuration was used: a ΔE (1 mm)-$E1$ (1 mm)-$E2$ (5 mm, which was tilted to $45°$). Because of the need for tilting and given the physical dimensions of the detectors, they were mounted behind a 3×5 mm collimator. Measurements were performed at small angles ($0°$, $5°$, and $10°$ in the laboratory) to maximize the counting statistics. To achieve reasonable angular resolution and separation between the primary beam and the reaction products while using the thinner target, the main telescope was mounted about 16 cm away from the target on one of the movable arms. The decision to focus on small angles forced us to introduce an additional 3×5 mm collimator before the target. A ΔE (40 μm)-E(700 μm) telescope for beam intensity measurements and tuning was mounted in the second arm about 14.8 cm away from the target at $20°$. The master triggers of the data acquisition system were either (a) the $E1$ detector or (b) a logical AND of the monitoring ΔE-E detectors. The detectors in the main telescope were separately calibrated with α sources (^{239}Pu, ^{241}Am, and ^{244}Cm) and collectively calibrated with elastically scattered protons (at the incident beam energy) and the $^{12}C+p$ elastic resonance scattering. The experimental energy resolution within this excitation energy interval was about 40 keV in the center-of-mass (c.m.) frame.

D. Results

To illustrate the quality of the experimental data, Fig. 1(a) presents the measured proton spectrum for the 2.2- to
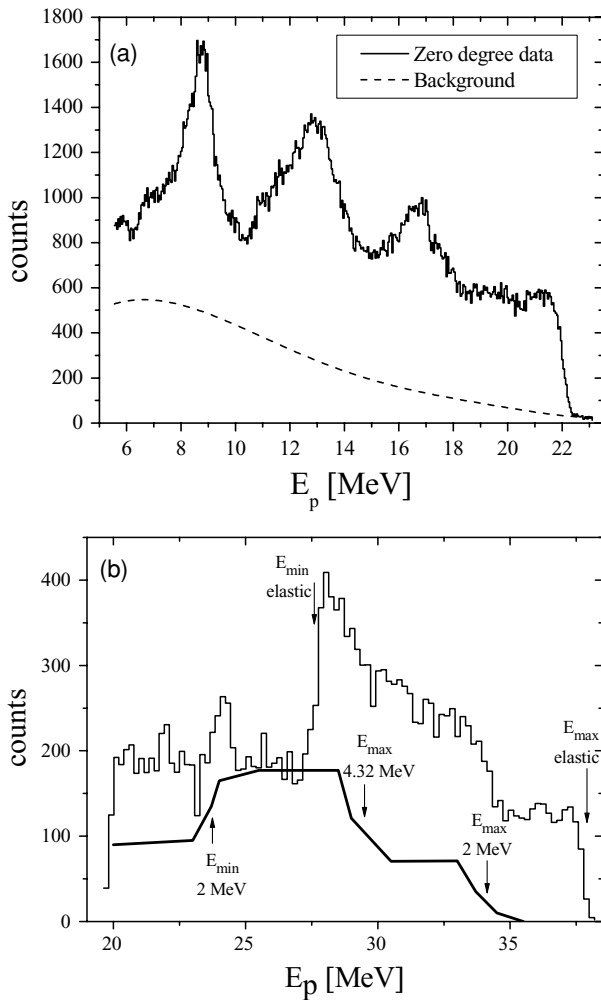
FIG. 1. (a) The experimental proton spectrum from ^{11}C$+p$ at an incident energy of $\sim$73.8 MeV for the 2.2- to 6.6-MeV excitation energy interval measured at 0° in the laboratory; the estimated proton background from the summed ^{11}C$+^{nat}$Ni and ^{11}C$+^{nat}$C reaction is also shown. (b) The experimental proton spectrum from ^{11}C$+p$ at 125 MeV for the 8.3- to 11.0-MeV excitation energy interval measured at 5° in the laboratory. The ^{11}C$+^{nat}$C background subtraction has already been done. The calculated contribution from the direct inelastic scattering is also shown (bold line). Only the population of the two lowest excited states of ^{11}C is assumed. (See text.)

6.6-MeV excitation energy interval. It also shows the estimated proton background originating from ^{11}C reactions with the Ni degrader and the ^{nat}C component of the polyethylene target. The ^{11}C$+^{nat}$Ni and ^{11}C$+^{nat}$C induced backgrounds were not investigated separately because the total background had been found to be smooth, i.e., all resonant structures are related to ^{11}C$+p$ interactions. (However, this leaves some uncertainty in the corresponding proton background.)

Because of the smoothness of the background data, statistical fluctuations between neighboring channels were removed by performing a polynomial fit to the data. (It is actually such a fit that is shown in Fig. 1(a).) The absolute position for the background spectra (in comparison to the main spectra) was determined by matching the high-energy tail of the proton spectra (only protons with energies higher than the ones possible from the ^{11}C$+p$ elastic resonance scattering were used). After such matching, the background subtraction was done from the measured proton spectra. An example of a background subtracted spectrum at high energy is given in Fig. 1(b) (see further discussion in Sec. IV).

The specific energy losses of ^{11}C and protons in (CH$_2$)$_n$ are needed to convert the number of events into relative elastic cross sections. These were computed using SRIM [17]. The relative cross sections were then converted to absolute ones using the data of reference [6] and the gas target data of the present work. Uncertainties related to the absolute normalizations are not included in the given error bars.

III. EXPERIMENTAL SETUP AND RESULTS AT TEXAS A&M UNIVERSITY

A. The ^{11}C beam and the setup for the 2.0- to 8.6-MeV excitation energy interval

At TAMU a ^{11}B beam of 0.3 μA was accelerated by the K500 superconducting cyclotron to 11.9 MeV/nucleon. This beam bombarded a hydrogen gas target of 9 cm length at liquid nitrogen temperature and 1.9 atm pressure with 4 μm Havar entrance and exit windows. The recoil spectrometer MARS [12] was used to filter the reaction products and provide a ^{11}C secondary beam, with a beam purity of 99.9%. Excitation functions for ^{11}C$+p$ elastic scattering were measured in a scattering chamber filled with methane (CH$_4$) gas that was placed at the MARS focal plane (see Fig. 2). A parallel plate avalanche counter (PPAC) was placed in the front of the entrance to this scattering chamber. The efficiency of the PPAC was about 100% at a ^{11}C beam intensity of 5×10^4 ions/s. The PPAC was used to find the ratio between the primary and the secondary beam and to estimate the cross sections at low beam intensity. (At the working intensity of the ^{11}C beam of 10^6 ions/s, the efficiency of the PPAC was only a few percent but could be reliably scaled to monitor the beam intensity.)

The ^{11}C radioactive beam entered the scattering chamber through a 12-μm organic (Aramica) foil; the ^{11}C beam energy after the foil was 99.8 MeV with an energy spread of 1.1% (full width at half maximum; FWHM). The 50-cm-long chamber was filled with methane gas of 99.0% purity at a pressure of 1 atm. The gas pressure was adjusted so that the beam stopped before the detector setup. Due to the large difference in energy loss, the recoiling protons, created by the elastic scattering of ^{11}C on hydrogen, penetrated through the gas into an array of ΔE-E Si detectors.

Four detector telescopes were positioned at 0°, -12.5°, $+11.5$°, and $+16.5$° relative to the beam direction. The ΔE detectors had thicknesses in the range of 75–100 μm. The zero degree telescope had a large (40-mm) circular aperture and a Si (Li) E detector that had an original manufactured thickness of 3.6 mm. As was found after the run, the thickness of the Si (Li) layer became much thinner with age, decreasing with the distance from the center. Therefore the spectra at 0° were only used to compare absolute cross section at low proton
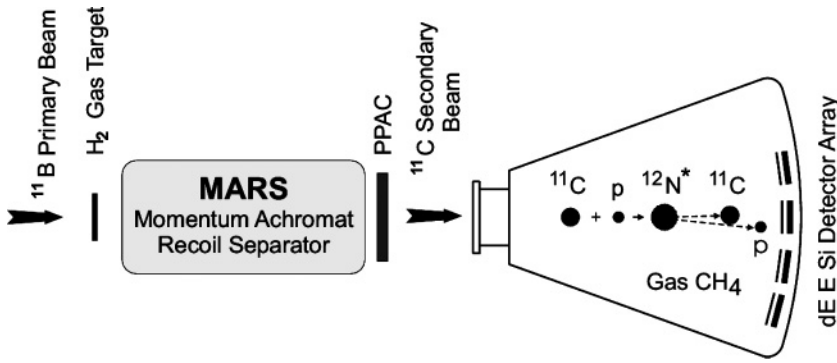
FIG. 2. A schematic drawing of the setup used at Texas A & M University.

energy with these of Ref. [6] and for qualitative information at somewhat higher energy (see Sec. VI B). All the other E detectors had a thickness of 5 mm, which was enough to stop 30-MeV protons.

Particle identification of the recoil protons was made by the ΔE-E method and the proton background from $^{11}C+^{nat}C$ reactions was evaluated using a Teflon target. This target was placed one-third of the way from the window of the scattering chamber to the detector plane but closer to the window. The proton background from reactions with ^{nat}C at $0°$ was negligible at proton energies over 2.5 MeV in the c.m. system. A different background behavior in comparison to the LBNL solid target data is an evident result of the two times higher concentration of hydrogen in the (CH$_4$) target and from the use of a low-density gas target. The background protons were mainly created by the high-energy part of the ^{11}C beam relatively far from the detectors. Therefore, the solid angle covered by the detectors for the background protons is considerably smaller in comparison to the solid target measurements. No background subtraction was introduced for the data at other angles. Note that the actual detection angle changes as a function of ^{11}C beam energy for the non-0° telescopes, as shown in Fig. 2. The experimental resolutions of the detectors were about 50 keV and the absolute calibrations were better than ± 25 keV in the c.m. system. Generally the experimental setup was similar to that used in Ref. [18].

B. Results

A few hours of gas target measurements were complementary to the solid target measurements discussed above. To improve the counting statistics the experimental points were summed over an energy of 30 keV in the c.m. system. These data were used to obtain the absolute values of the cross sections with a precision better than 15% at angles other than 0° and to test the fit at large angles. The gas target data also provided a test of the importance of resonance inelastic scattering (see Sec. IV). This arises because the inelastic scattering should occur at higher incident energy than the elastic scattering to produce protons with the same energy. Based on similar solid angle arguments to those discussed earlier in the context of the background protons, the gas target also efficiently suppressed any inelastic component in the scattering.

IV. INELASTIC SCATTERING BACKGROUND

Because the proton background that results from inelastic scattering cannot be eliminated in these experimental setups, this background deserves special discussion. At the highest beam energies, $\sim$10 MeV/nucleon, the excitation of the lowest excited states of ^{11}C can proceed via a direct reaction mechanism, thereby generating a significant smooth proton background. (However, such a background should be negligible in comparison with the strong elastic scattering resonances at lower ^{11}C energies, $\sim$5 MeV/nucleon.) In addition, resonance inelastic scattering (RIS) may be important at the higher energies. In the TTIK technique, peaks arising from RIS can be easily mistaken for resonance elastic scattering (RES). The condition producing the strongest resonances in the inelastic scattering occurs when the partial widths for the decay to the ground state and to the excited state are relatively close to one another. This means that the corresponding RES should also be observed as a strong resonance. However, in measurements at small angles, if only the RES is assumed in the analysis the possible RIS component can manifest itself in the data as stronger resonances compared to RES. This happens because (a) the inelastic scattering occurs at higher energy and smaller specific energy loss than the corresponding elastic scattering and (b) the effective solid angle in the laboratory system is larger for the inelastic scattering (the maximum angle for the protons in RIS is less than 90°).

To study the role of inelastic scattering in the solid target data, we made measurements using a relatively thin (CH$_2$)$_n$ target (20.2 mg/cm^2) and the 125-MeV ^{11}C beam. Figure 1(b) presents the 5° spectrum in the laboratory system. The arrows show the characteristic energies related to the possible population of the first and second excited states in ^{11}C (2.00 and 4.32 MeV). Only inelastic scattering can be responsible for proton energies less than 28 MeV. There is a flat part and a peak in this region. The flat part corresponds to $\sim$15 mb/sr c.m. cross section near 25.5 MeV, which is in good agreement with $\sim$16 mb/sr cross section observed for the sum of the population of the lowest excited states in the inelastic scattering of 9.7-MeV neutrons on ^{11}B at 150° [19]. It appears to be reasonable to relate the flat part with the mechanism of direct inelastic scattering. The peak at the proton energy of $\sim$24.2 MeV would correspond to a c.m. cross section of $\sim$15 mb/sr if it were taken to be an elastic-scattering resonance. However, the peak must arise from RIS, and its population corresponds to less than 8 mb/sr. If this peak corresponds to

the population of the first excited state in ^{11}C (2.0 MeV; 1/2$^-$), the resonance is at $\sim$8.2 MeV excitation energy in ^{12}N; if it is excitation of the second excited state in ^{11}C (4.3 MeV; 5/2$^-$), the resonance corresponds to $\sim$9.7 MeV excitation energy. Close to both of these energies we have observed resonances in the elastic-scattering data (see Sec. VI E below). We are inclined to relate this peak to the state at 8.2 MeV, because the low-energy side of the peak matches the low-energy cutoff of the elastic scattering and because the data of [Ref. [2]] (Fig. 4)] observe the state at 8.4 MeV in ^{12}N to decay to the first excited state in ^{11}C.

Assuming energy independence of the cross sections for direct inelastic scattering upon the c.m. energy in the region 7.7–10.4 MeV and using neutron scattering data [19] on the relative population of the lowest excited states, one can extrapolate the contribution of the inelastic scattering from the 25.5-MeV proton energy region to lower and higher energies. The bold curve in Fig. 1(b) presents this extrapolation. As shown, inelastic scattering can be responsible for 20–30% of the counts at the highest energies. We did not subtract the direct inelastic scattering from the spectrum for the data analysis because of the lack of exact numbers that would be needed for the extrapolation, as well as because of our tentative results of the analysis at the highest energies (also see below).

As pointed out, the gas target data are less sensitive to the inelastic scattering. As an example, the peak under discussion, at 24 MeV, should be about two times smaller in comparison to the neighboring elastic-scattering peaks under the specific conditions of our gas target experiment. In addition, because of the design of the scattering chamber for the gas target experiment, a neck (shown but not in scale in Fig. 2) at the entrance window inhibited the observation of scattering in the neck (at high energies) by the non-0° detectors. That is also the reason for the high-energy cutoff at about 8-MeV c.m. energy in the gas target data.

V. R-MATRIX ANALYSIS AND THE GLOBAL DESCRIPTION OF THE RESULTS

Figure 3 shows the zero degree excitation function in the excitation energy range of ^{12}N from 2.2 to 5.9 MeV. (Note that 0° in the lab is 180° in the center of mass.) This part of our measurements possesses the best counting statistics and energy resolution. In addition, (a) any potential scattering is minimal at 0° and (b) the resonances are more prominent at this angle. As a result, the main goal of the calculations was to fit these data. The gas target data in Fig. 3 were shifted down in cross section to provide a clearer view of the solid target results. Although the cross section for the dominant peak at 3.1 MeV excitation from the gas target data agrees fairly well with that from the solid target data, the gas target data at 0° are distorted, especially at higher energies (not shown in Fig. 3), for reasons given earlier.

As shown in Figs. 3, 4, and 5, the excitation functions do not produce sharp, strong, separated peaks, and, as can be understood from the level schemes shown in Fig. 6, several states can contribute to each broad bump in the spectra. The ^{11}C spin, 3/2$^-$, together with the proton spin, generates two possible spin channels ($S = 1, 2$). Further, in many cases,
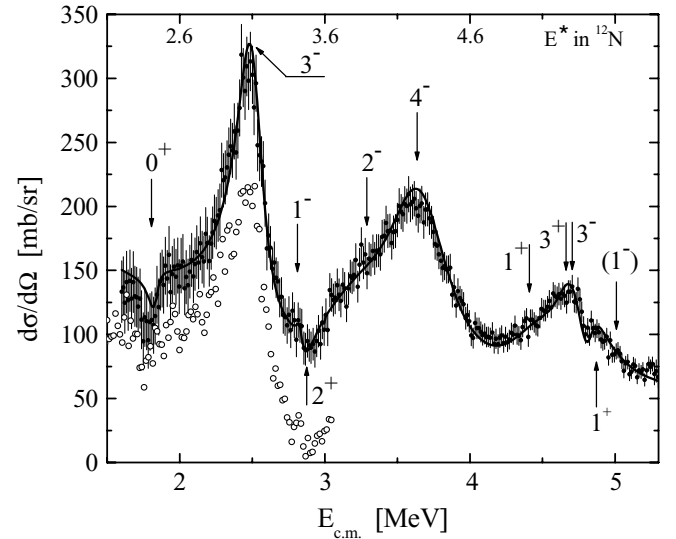

FIG. 3. The zero degree solid target c.m. excitation function and the corresponding R-matrix fit. Zero-degree gas target data (open circles) are also shown. Note that for clarity, the gas target spectrum is shifted down in cross section by a constant amount of 50 mb/sr. Excitation energy E^* is $E_{c.m.}$+0.601 MeV.

at least two orbital angular momenta can contribute to a resonance. In addition, the proton decay threshold in ^{12}N is low (0.601 MeV), and the excitation energy of the first excited state in the daughter nucleus, ^{11}C, is also rather low, 2.0 MeV. This leads to the expectation that many of the low-lying single-particle states in ^{12}N should be broad and thereby influence large regions of the excitation function. Many parameters are needed to describe this situation in the framework of the R-matrix model [20]. These are the spin, the excitation energy and the total width of the resonance, two amplitudes for the population of the spin channels for each orbital angular momentum value (the relative sign between the amplitudes is also important), and the R-matrix radius parameter. The large number of parameters makes this analysis very difficult and also potentially unreliable, especially at the higher excitation energies.

Fortunately, there are also some simplifying factors related to a resonance investigation of ^{12}N (as well as other drip line nuclei): because of the low binding energy of the last proton, an excitation function can be measured for relatively low-lying levels. Contemporary calculations using various shell-model (SM) [21,22] approaches are reliable for these low-lying states, and, in addition, many corresponding levels are known in the mirror nucleus ^{12}B, which is experimentally more accessible. Introducing such available information directly into the R-matrix code (as is explained below) was important in our analysis.

The analysis of the ^{11}C+p excitation functions was made in the framework of a complete R-matrix approach [20,23]. This means that the code took into account relevant nuclear structure and the different possible decay modes of the ^{12}N levels, as well as providing a correct calculation of the contributions of levels with the same spin and parity. The procedure used to fit the region from 2.2 to 5.6 MeV in excitation energy was the
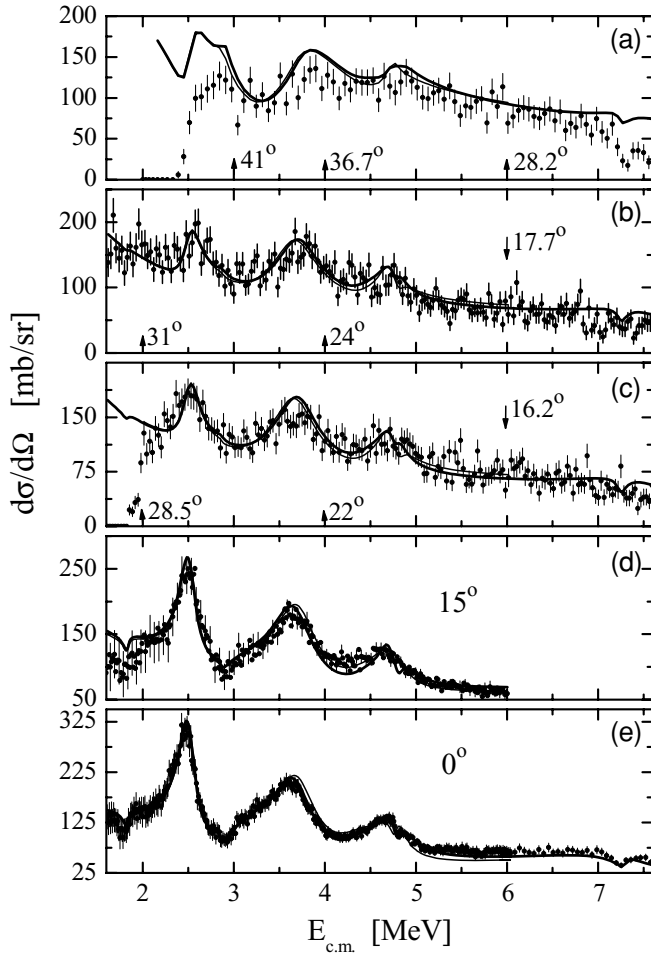
FIG. 4. The c.m. excitation functions for the ^{11}C+p elastic resonance scattering from 2.2 to 8.2 MeV. R-matrix fits were calculated based on the 0° data (bold line) and on the 15° data (thin line) and the parameters of these fits were used to calculate excitation functions at the other angles. (a) +16.5° gas target data; (b) −12.5° gas target data; (c) +11.5° gas target data; (d) 15° solid target data; and (e) 0° solid target data. To convert the $E_{c.m.}$ energy scales to excitation energies, 0.601 MeV should be added to them. Note that in the case of the gas target data, the actual detection angle changes as a function of the ^{11}C beam energy.

FIG. 5. The excitation function for ^{11}C+p elastic resonance scattering from 6.6 to 11.0 MeV, measured using the ΔE-E_1-E_2 telescope (a) at 10°; (b) at 5°; and (c) at 0°. Also shown are the conventional (dashed line) and modified/final (solid line) R-matrix fit to the 0° data. (See text.)

following: (1) for the known levels of ^{12}N the initial parameters were taken from Refs. [1,3,6]; see also Table I. The parameters for these levels were not allowed much variation. (2) All levels that are known in ^{12}B (up to 6.6 MeV, see Fig. 6) but were unknown in ^{12}N, were considered in the following way. A comparison of excitation energies of well-known levels in ^{12}B and ^{12}N [1,3,6] shows that the mirror levels in ^{12}N are typically lower than in ^{12}B by about 200 keV. Note, however, that this shift can be as large as 800 keV for levels corresponding to a 2s single-particle configuration, because of the Thomas-Ehrman effect (for details see Ref. [3]). If the excitation energies of the ^{12}N levels were poorly defined or unknown, this 200-keV shift was used to specify initial values for these excitation energies. In the fitting procedure these input excitation energies were allowed to vary by ±500 keV.
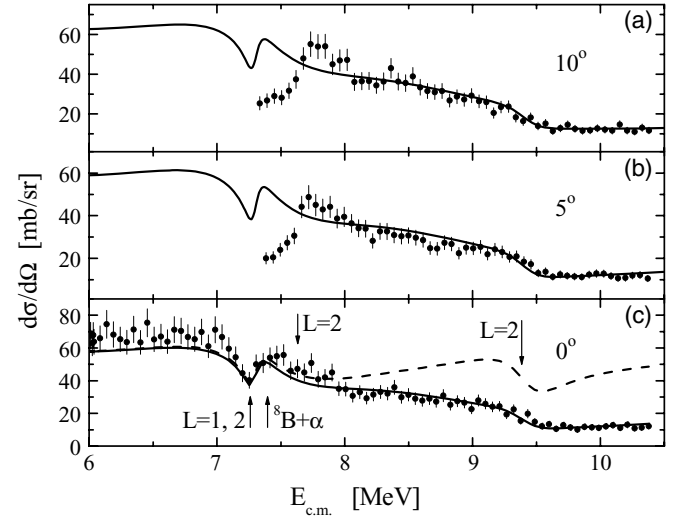
Then, (3) the initial values for the widths of the states in ^{12}N (if unknown) were obtained using the widths of the corresponding levels in ^{12}B. Note that the ^{12}B level widths from 3.37 to 5.49 MeV in excitation energy are mainly defined by neutron decay to the ground state of ^{11}B. The level widths in ^{12}B were converted to ^{12}N-level widths by means of a potential model [18] (see details below) and used as initial parameters for the proton decay partial widths to the ground state of ^{11}C. The values obtained in this way were allowed to vary within a factor of 2. (4) The nuclear structure of the levels was assumed to be given by the SM predictions [21,22]. This assumption then specified the coefficients in the spin-channel representation. These coefficients for the spin-channel R-matrix representation for each l orbit were taken to be proportional to the Racah transformation coefficients between the two coupling schemes of ($I_1 + I_2 = S$; $S + l = J$) and ($l + I_2 = j$; $I_1 + j = J$), where I_1, I_2, and J are the spins of the ^{11}C, p, and the resonance state in ^{12}N and S is the channel spin. In cases where two orbital angular momenta contribute, the sign between the wave functions was taken from the SM calculations. This adopted sign was tested in the fitting process. As is clear, the above procedure opens a way to test the detailed SM predictions. However, it is important to stress that the SM is dealing with spectroscopic factors, whereas the reduced widths are defined in the R-matrix calculations. Therefore, additional assumptions need to be made for the direct comparison of these entities. We can characterize only qualitative features of these predictions in the present approach.

For this analysis, the width of a resonance was defined as the difference between the energies at which the square of the absolute value of the first element (1,1) of the matrix (the notation is the same as in Ref. [20]), $1/k\,P^{1/2}(1-RL)^{-1}R\,P^{1/2}$, equals 1/2 of its maximum value at the resonance energy. The R-matrix in this case was truncated to include only one resonance.

STRUCTURE OF ^{12}N USING ^{11}C$+p$ RESONANCE SCATTERING

PHYSICAL REVIEW C **74**, 024306 (2006)

TABLE I. The energies, spins and parities, and widths of the levels of ^{12}N.

Present work			Ref. [1] (Ajzenberg-Selove)			Ref. [2] (Harakeh et al.)		Ref. [3] (Anderson et al.)			Ref. [6] (Teranishi et al.)	
E_{ex} (MeV)	J^π	Γ (MeV)	E_{ex} (MeV)	J^π	Γ (MeV)	E_{ex} (MeV)	J^π	E_{ex} (MeV)	J^π	Γ (MeV)	E_{ex} (MeV)	J^π
			0.960(12)	2^+	<0.020							
1.195	2^-	0.109	1.191(8)	2^-	0.118(14)			1	$2^+, 2^-$			
1.796	1^-	0.581	1.800(30)	1^-	0.750(250)			1.8	1^-			
2.428	0^+	0.079	2.439(9)	0^+	0.068(21)							
3.120		0.225										
(3.127)	3^-	(0.227)	3.132(8)	$2^+, 3^-$	0.220(20)			3.2	(3^-)		3.1	3^-
3.433	1^-	0.052										
3.480		0.201										
(3.480)	2^+	(0.211)	3.558(9)	$(1)^+$	0.220(25)			3.5	$(1^-, 2^+)$		3.6	$(2)^+$
3.924		1.040										
(3.983)	2^-	(1.056)	4.140(10)	2^-+4^-	0.825(25)			4.18(5)	2^-	0.836(25)		
4.300		0.587										
(4.340)	4^-	(0.572)						4.41(5)	4^-	0.744(25)		
5.062		0.433										
(5.015)	1^+	(0.445)										
5.370		0.534										
(5.275)	3^+	(0.490)										
5.393		0.415										
(5.331)	3^-	(0.480)	5.348(13)	3^-	0.180(23)			5.40(5)	$3^+, 3^-$	0.385(55)		
5.451		0.180										
(5.410)	1^+	(0.207)										
[5.600]		[1.658]										
[(5.500)]	$[(1^-)]$	[(1.696)]										
			(5.600(11))		0.120(50)							
			6.400(30)	(1^-)	1.200(30)	6.4	(2^-)	6.4	1^-			
			7.400(50)	(1^-)	1200(30)	7.4	(1^-)	7.3	1^-			
			7.684(21)		0.200(32)							
7.831	$(1^-, 2^+)$	0.078										
8.200	$(1^-, 2^-, 3^-)$	1.270						8.2	(1^-)			
			8.446(17)		0.090(30)							
			9.035(12)		<0.035							
			(9.420(100))		~0.200							
10.026	(3^-)	0.605	9.800(20)		0.450(100)	9.9	(0^-)	10.0	(1^-)			
			10.300(20)		0.450(100)							
			11.000(20)		0.350(100)							

Conclusions concerning the possible resonance states above 5.6 MeV excitation energy are speculative since the theoretical predictions in this region are inaccurate due to the truncation of the shell-model space and also because of the lack of supporting experimental data. In the R-matrix fit of the data their properties were allowed to vary the same way as described above. More specific details are given in the next section.

After initializing the parameters, as explained above, a fit to the 0° solid target data was made (see Figs. 3, 4(e), and 5(c)). The spins of the weaker and more uncertain resonances were varied. An inspection by eye was a necessity in the initial steps of the fitting procedure because of the large number of local minima.

The parameters of the fit to the 0° data were then used to calculate excitation functions at other angles. Figure 4 presents our experimental data and the R-matrix calculations in the excitation energy range of 2.2 to 8.2 MeV. As can be seen in Fig. 4, the measurements cover the angular interval from zero up to ~40° (from 180° to ~100° in the c.m. system) for the lowest excitation energies. Though the general character of the excitation functions appears to be relatively stable with angle, for the cases where many spin projections are involved, some changes can be seen. These changes include the variation of the amplitudes of the maxima; an increase of the cross section with angle at the flat high-energy part; and a shift of maxima to higher excitation energy with angle (within their widths). The last is a result of a complicated interference between the resonances and the potential scattering. All of these changes are described by the calculations with the same set of parameters.
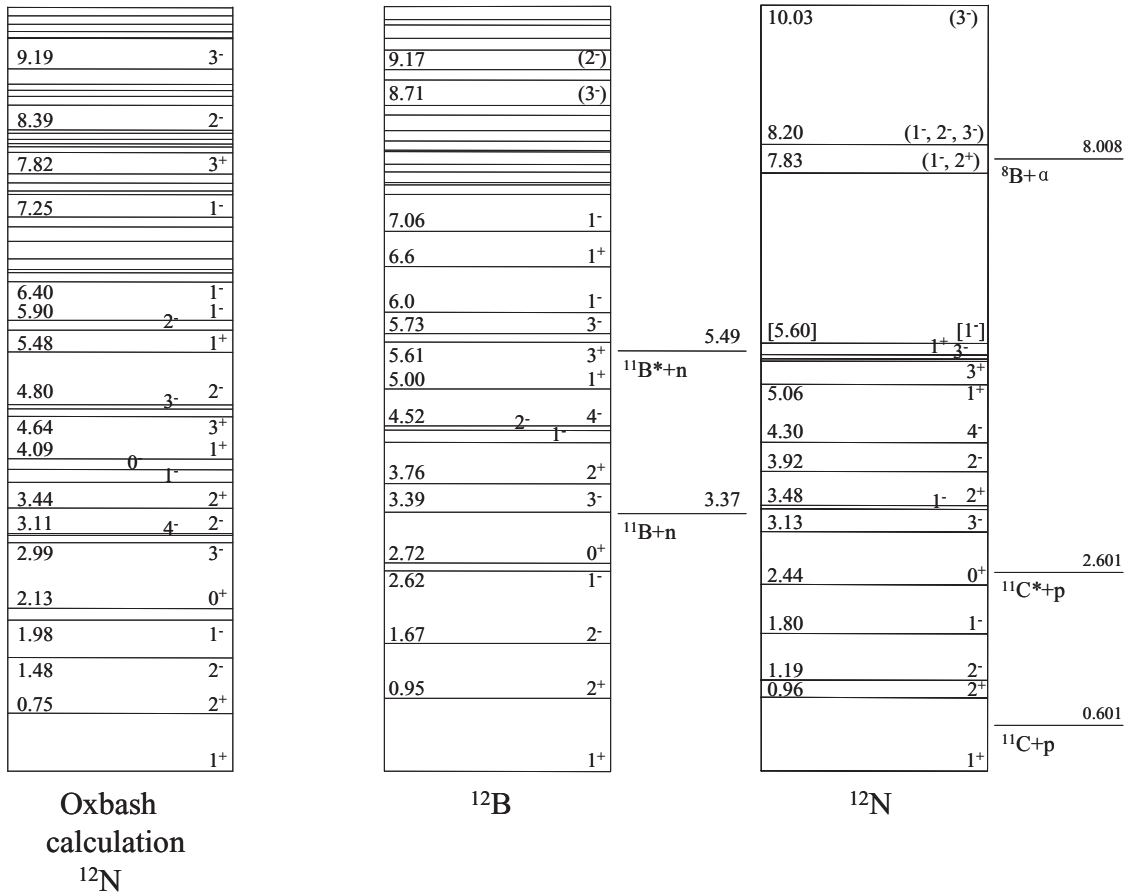
FIG. 6. The shell-model ^{12}N and experimental ^{12}B and ^{12}N (present work) level schemes. Earlier data (see text) are displayed for the lowest-lying states of ^{12}N. The ^{12}B data are from Ref. [1].

Given that the level structure of ^{12}N involves many broad and overlapping levels, we prefer not to assign error bars to the energies and level widths of the states that have been fitted. However, the following analysis can serve as a guide to the stability of the results below 5.6 MeV excitation energy: As shown in Fig. 4(d), the fit to the 15° solid target data using the parameters from the 0° fit is not perfect (bold line). (One should, however, note that the 15° data were collected under nonoptimized experimental conditions, i.e., the ^{11}C beam was not perfectly focused.) We then adjusted the parameters to obtain a better description of the 15° solid target data (the thin line in Fig. 4). The differences between the parameters of the fit to the 0° and to the 15° data can then be taken as an estimation of the overall precision and stability of the results. The most evident differences are a shift of the 3$^+$ level energy by about 95 keV and the increase of the width of the nearby 3$^-$ level by about 16%. The energies and level widths from the adjusted fit for the levels from 3.1 to 5.6 MeV are given in parentheses in Table I.

One can see that the calculated cross sections in Fig. 4(e) are systematically slightly lower than the 0° solid target data in the region of 5- to 7-MeV c.m. energy. This difference may be attributed to a larger contribution of the direct inelastic scattering to the measurements with a solid target (see also Figs. 4(a) to 4(c)).

We found during the fitting procedure that the R-matrix calculations generated larger cross sections than the measured ones at the highest energy part of our spectra; in addition, this discrepancy increased with energy, see Fig. 5(c) (dashed line). In this energy region the resonances are relatively weak, and a dominant contribution to the cross section comes from potential scattering. We can relate the discrepancy to the increased role of direct reactions, which is not taken into account in the R-matrix code. The general recommendation for incorporating this effect in the R-matrix formalism is via implementation of some hypothetical faraway resonances [20]. However, we decided that it was more convenient to add imaginary phase shifts to the phase shifts generated by the R-matrix calculations; these imaginary phase shifts were calculated in accordance with the following phenomenological expression:

$$\mathrm{Im}\delta_l(k) = A \left(1 - \frac{1}{1 + e^{(kR-l)/A_1}} \right) \left(1 - \frac{1}{1 + e^{(kR-l_0)/A_2}} \right) \tag{1}$$

where $A = 0.35$, $A_1 = 0.2$, $l_0 = 2.9$, and $A_2 = 0.1$ are constants. This parametrization provides for the rapid rise of imaginary phase shifts from the very small values at energies less than 6 MeV up to 0.35 at 11 MeV. This value, 0.35 for 11 MeV, is in good agreement with the one generated by the optical model using conventional parameters [24]. The strong

dependence on l leads to negligible phase shifts for orbital momenta greater than 4. Figure 5(c) (solid line) presents the improved/final fit to the high-energy 0° data.

As can be seen in Figs. 4 and 5, though only the 0° data were considered in the fitting procedure, the fits are reasonably good at all angles, including the gas target measurements. The χ^2 values are in the region of 0.8–1.5 per degree of freedom for all angles in the excitation region in question. No corrections related to the experimental energy resolution or the angular acceptances were introduced into the calculations, because it was found that they had negligible effect in the region of interest. The resonance parameters resulting from this R-matrix analysis are given in Table I.

VI. RESONANCES

A. The lowest levels (0.96, 1.19, 1.80, and 2.44 MeV, from Ref. [1])

The known narrow 2^+ level at 0.96 MeV and the 2^- level at 1.19 MeV are below the excitation region investigated. However, the presence of the 2^- level influences the fit. The parameters of this level were taken from Ref. [1] and are in agreement with a pure $2s_{1/2}$ state assignment. The broad 1^- state at 1.80 MeV affects even more the region of interest. However, the final fit suggests a smaller width than the adopted one (see Table I), but it still lies well within the quoted error bars. The width of the narrow 0^+ state at 2.44 MeV (see Fig. 3) was considered to be related to a $p_{3/2}$ single-particle configuration, as predicted by the SM. The excitation energy found for this state agrees well with the known value [1]. This agreement, together with a similar conclusion for the 3.13-MeV state (see below), confirms the correctness of the steps taken during the energy calibration of the lower-energy 0° data. The slight deviation between the experimental and calculated cross sections for the lowest energies in the 0° data probably results from an inexact proton background subtraction (see Sec. II D). However, some low-energy cutoff effects cannot be completely excluded.

B. The 3.13-, 3.43-, and 3.48-MeV levels (from this work)

The peak at 3.13 MeV [1] (see Figs. 3 and 4) is easily identified as a 3^- resonance because of its large cross section and a strong dependence of the excitation cross section on angle. This assignment agrees with Ref. [6], in which measurements were made only at 0° by the same method as employed in the LBNL data. The mirror state in ^{12}B is at 3.39 MeV and is the first level in ^{12}B decaying by neutron emission, with a width of 3.1 ± 0.6 eV [1]. A calculation using a Woods-Saxon potential [18] ($r_0 = r_C = r_{SO} = 1.22$ fm; $a = 0.6$ fm; $V_{SO} = 6.0$ MeV), with a well depth adjusted to reproduce the separation energy of a neutron from the 3.39 MeV state in ^{12}B, predicts the excitation energy of its mirror state in ^{12}N with better than 100-keV precision. The width of this 3^- state in ^{12}N is known to be 220 ± 20 keV [1] (see also Table I). This width is mostly expected to be related to decay to the ^{11}C ground state and it would lead to a $5.5 \pm$

0.5 eV neutron width for the corresponding mirror state in ^{12}B. A change in the Coulomb radius (r_C) from 1.22 to 1.26 fm results in only a 1% change in the width of the 3^- state in ^{12}N. This disagreement with the tabulated width for the 3^- state in ^{12}B implies that it should be reconsidered.

For the 3.43-MeV, 1^- state, there is a small peculiarity within this energy region, that manifests itself as a narrow peak in the gas target data; see Fig. 3 (open circles). The inclusion of an 1^- state with a small $d_{5/2}$ amplitude and a much higher amplitude for the $l = 0$ decay to the first excited state ($1/2^-$) in ^{11}C fits the data. The excitation energy for this state is in perfect agreement with the prediction of 3.449 MeV [3] based on the mirror structure of ^{12}B and ^{12}N. Also, a narrow width agrees with the 9-keV width of the mirror state in ^{12}B, where the only possible decay is to the ground state of ^{11}B. It is worthwhile to note that the dominant coupling to the first excited state in ^{11}C is in fair agreement with the qualitative predictions of the SM for this level. However, the predicted value for the $d_{5/2}$ strength is 10 times smaller than the experimental value.

For the 3.48 MeV, 2^+ state, there is a minimum at 3.48 MeV excitation energy whose shape corresponds to a $l = 1$ resonance. A tentative assignment, (2^+), was given for this state in Ref. [6]. The amplitude of the minimum and the width of the resonance imply a very small (less than 6%) decay into the first excited state in ^{11}C. Therefore a 1^+ assignment can be rejected on the basis of cross-section considerations. A 3^+ assignment would need an unrealistically large component of a decay with $l = 3$ to the first excited state in ^{11}C. Therefore we assign the quantum numbers, 2^+, for this level at 3.48 MeV in excitation energy. In ^{12}B this 2^+ state lies at 3.76 MeV (see Fig. 6).

C. The 3.92- and 4.30-MeV levels (from this work)

The known 2^- and 4^- levels [3] should contribute to the broad and strong group seen at about 4.3 MeV in excitation energy in Fig. 3. The large cross section related to this structure suggests $l = 2$ and indeed both resonances seem to contribute to it. The orbital momentum $l = 2$ (a $d_{5/2}$ single-particle configuration) is the only choice for the 4^- resonance ($l = 4$ is hindered because of nuclear structure and penetrability considerations). As for the 2^- resonance, the SM predicts both large $d_{5/2}$ structure and $2s$ structure. (It is possible—but in disagreement with the theoretical predictions—to fit the 0° excitation function with a single $2s$ structure for the 2^- resonance. However, this worsens the agreement at larger angles.)

As shown in Table I, there is only moderate agreement between the present data and those of Ref. [3] for the level energies and widths of the 2^- and 4^- states. The width of the mirror 4^- state in ^{12}B is 110 ± 20 keV [1]. A similar potential well calculation to that described earlier gives about 600 keV for the 4^- state in ^{12}N. (It is unlikely that the additional open channel of a decay to the first excited state in ^{11}C with $l = 4$ and a 1000 times smaller penetrability could influence this result.) Our result for the width of the ^{12}N 4^- state (590 keV) agrees well with this 600-keV estimation. No similar comparison can be made for the 2^- state because the width of the mirror state in ^{12}B is given only as "broad" in the compilation [1]. Note that

decays with $l = 2$ and $l = 0$ both contribute to the 1.04-MeV width of the state. (Interestingly, the sum of the widths for these 2^- and 4^- states is similar in both the present work and that of Ref. [3].)

D. The 5.06-, 5.37-, 5.39-, and 5.45-MeV levels (from this work)

Based on the ^{12}B level scheme, several states can contribute to the cross section near the 4.7 MeV c.m. energy bump. The fit was made using the 1^+, 3^+, and 3^- levels in agreement with the level scheme of ^{12}B and the SM calculations. The value of the cross section in the peak indicates the presence of a resonance with an orbital angular momentum as high as $l = 2$ (the 3^- resonance). As for the 1^+ and 3^+ resonances, their influence is similar. They are not so prominent, but they do provide the observed cross-section behavior between the bumps at 3.7 and 4.7 MeV c.m. energy and they also define correctly the nearby slopes of the bumps. Note, however, that the widths of all three of these states are larger than their counterparts in ^{12}B (they are about a factor of 2 larger than would be expected after taking the penetrability into account).

A small dip at 4.8 MeV c.m. energy, see Fig. 3, as well as the falloff after the bump was fitted by inclusion of a narrow 1^+ resonance ($\Gamma = 180$ keV) at 5.45 MeV excitation. Quite probably the mirror level in ^{12}B is the state at 6.6 MeV excitation energy ($\Gamma = 140$ keV) [1]. The shell-model calculations (Fig. 6) predict a 1^+ level at 5.48 MeV.

E. Levels above 5.45 MeV

The 0° excitation function is flat between 5 and 7 MeV c.m. energy. The R-matrix calculations reproduce this plateau but with slightly smaller cross sections. We tried to improve the fit within this energy region by introducing a broad 1^- state at 5.6 MeV (a possible mirror of the 6.0 MeV state in ^{12}B; see Fig. 6). However, varying the parameters of this resonance produced only minor improvements to the fit. As a result, this analysis can only be considered to provide weak evidence for such a state (see also the relevant discussion in Sec. V).

At higher energies the data on the ^{12}B levels are rather scarce and the SM predictions become unreliable. Some naive shell-model considerations (also supported by the real SM calculations) suggest that relatively strong resonances could be related to the $d_{3/2}$ strength. Indeed two "steps" in the excitation function at 7.6 and 9.4 MeV c.m. energy can be fitted with a dominant $d_{3/2}$ contribution (see Fig. 5). The 7.6-MeV resonance corresponds to 8.2-MeV excitation energy. There are several 3^- levels in ^{12}B near this energy but they are all rather narrow. The quantum characteristics of the broad 8.1-MeV level in ^{12}B are not known. There are also no obvious candidates in ^{12}B to compare with the 10-MeV level. Reference [3] proposes 1^- states at 8.2 and 10 MeV in ^{12}N ($\Gamma = 1.2$ MeV for both states).

There is a sharp interference dip near 7.23-MeV c.m. energy. Because the resonance is weak and sharp, it is likely a low-spin state. An equally good fit could be obtained for a 1^- or a 2^+ state. There are two narrow 1^- levels near the 7.8-MeV

excitation region in ^{12}B, 7.84 and 7.94 MeV. It might be that the resonance found in ^{12}N corresponds to one of these.

There is an astrophysical interest in resonances in the energy region near 8 MeV because of their proximity to the ^{8}B$+\alpha$ (8.008 MeV) threshold. The resonance capture of α-particles could markedly increase the rate of ^{11}C production via the ^{8}B$+\alpha \rightarrow {}^{11}C+p$ reaction. The influence of a resonance on the ^{11}C production rate depends on its α-partial width; however, the α-partial width will always be relatively small because of its low penetrability. Related to this, a 2^+ resonance spin-parity would be important to permit α-particle capture with zero orbital angular momentum. The 7.8-MeV resonance is the only level that we observed near this threshold with a possible 2^+ spin-parity. However, despite the fact that our energy calibration worsens at higher energies, it is unlikely that this level could be about 200 keV higher in energy. It is worthwhile to note that the nonobservation of such a suitable level in the present work does not mean that it cannot exist. There is still the possibility that a resonance in the ^{8}B$+\alpha$ interaction could be coupled with proton decay to an excited state of ^{11}C.

VII. SUMMARY

We have measured the ^{11}C$+p$ elastic scattering in the excitation region of ^{12}N from 2.2 up to 11 MeV by the thick target inverse kinematics method. Measurements were made using both solid and gas targets. This combination gave us the possibility of studying the importance of inelastic scattering. The data were analyzed in the framework of the R-matrix approach, also using known data on ^{12}B levels and the predictions of the shell model(s). Sixteen levels were analyzed in ^{12}N, and data on their spin-parities, excitation energies, and widths are presented. For the four levels above 5.45 MeV excitation, only suggested parameters are given. A narrow state with a tentative low-spin assignment was found about 200 keV below the ^{8}B$+\alpha$ threshold in ^{12}N.

Conventional R-matrix calculations generated cross sections at the highest energies that were too large. We related this effect to the increasing role of direct reactions and took their influence into account by adding imaginary parts (parameterized by a simple expression) to the phase shifts generated by the hard sphere scattering. Generally, the SM predictions were a good guide for the analysis of the lowest excited states. However, at higher excitation energies, the spread of the $d_{3/2}$ strength appeared to be underestimated and the predicted dominant $d_{3/2}$ levels appeared to be shifted to lower energies.

[1] F. Ajzenberg-Selove, Nucl. Phys. **A506**, 1 (1990).

[2] M. N. Harakeh *et al.*, Nucl. Phys. **A577**, 57c (1994).

[3] B. D. Anderson, L. A. C. Garcia, D. J. Millener, D. M. Manley, A. R. Baldwin, A. Fazely, R. Madey, N. Tamimi, J. W. Watson, and C. C. Foster, Phys. Rev. C **54**, 237 (1996).

[4] A. Lefebvre *et al.*, Nucl. Phys. **A592**, 69 (1995).

[5] A. Galindo-Uribarri *et al.*, *Frontiers of Nuclear Structure* (American Institute of Physics, Woodbury, NY, 2003), Vol. 656, p. 323.

[6] T. Teranishi *et al.*, Phys. Lett. **B556**, 27 (2003).

[7] X. Tang, A. Azhari, C. A. Gagliardi, A. M. Mukhamedzhanov, F. Pirlepesov, L. Trache, R. E. Tribble, V. Burjan, V. Kroha, and F. Carstoiu, Phys. Rev. C **67**, 015804 (2003).

[8] W. Liu *et al.*, Nucl. Phys. **A728**, 275 (2003).

[9] M. Wiescher, J. Görres, S. Graff, L. Buchmann, and F.-K. Thielemann, Astrophys. J. **343**, 352 (1989).

[10] K. E. Rehm *et al.*, Nucl. Phys. **A746**, 354c (2004).

[11] J. Powell *et al.*, Nucl. Instrum. Methods A **455**, 452 (2000).

[12] R. E. Tribble, A. Azhari, C. A. Gagliardi, J. C. Hardy, A. Mukhamedzhanov, X. Tang, L. Trache, and S. J. Yennello, Nucl. Phys. **A701**, 278c (2002).

[13] Z. Q. Xie and C. M. Lyneis, Rev. Sci. Instrum. **67**, 886 (1996).

[14] H. Wollnik, Nucl. Instrum. Methods **139**, 311 (1976).

[15] F. Guo, Ph.D. thesis, University of California, Berkeley, 2004.

[16] K. P. Artemov *et al.*, Sov. J. Nucl. Phys. **52**, 408 (1990); V. Z. Goldberg, Clustering Phenomena in Atoms and Nuclei, edited by M. Brenner, T. Lönnroth, F. B. Malik (Springer, New York, 1992).

[17] http://www.srim.org

[18] V. Z. Goldberg, G. G. Chubarian, G. Tabacaru, L. Trache, R. E. Tribble, A. Aprahamian, G. V. Rogachev, B. B. Skorodumov, and X. D. Tang, Phys. Rev. C **69**, 031302(R) (2004).

[19] J. A. Cookson and J. G. Locke, Nucl. Phys. **A146**, 417 (1970).

[20] A. M. Lane and R. G. Thomas, Rev. Mod. Phys. **30**, 257 (1958).

[21] B. A. Brown, Prog. Part. Nucl. Phys. **47**, 517 (2001).

[22] A. Volya and V. Zelevinsky, Phys. Rev. Lett. **94**, 052501 (2005).

[23] G. V. Rogachev (private communication).

[24] A. Bohr and B. R. Mottelson, *Nuclear Structure* (Benjamin, New York, 1969), Vol. 1.